Nanoscale

PAPER

View Article Online
View Journal | View Issue

Cite this: *Nanoscale*, 2016, **8**, 5786

Three-dimensional WS_2 nanosheet networks for H_2O_2 produced for cell signaling†

Jing Tang,‡[a] Yingzhou Quan,‡[a] Yueyu Zhang,‡[b] Min Jiang,[c] Abdullah M. Al-Enizi,[d] Biao Kong,[a] Tiance An,[a] Wenshuo Wang,[e] Limin Xia,[e] Xingao Gong[b] and Gengfeng Zheng*[a]

Received 28th December 2015,
Accepted 8th February 2016

DOI: 10.1039/c5nr09236a

www.rsc.org/nanoscale

Hydrogen peroxide (H_2O_2) is an important molecular messenger for cellular signal transduction. The capability of direct probing of H_2O_2 in complex biological systems can offer potential for elucidating its manifold roles in living systems. Here we report the fabrication of three-dimensional (3D) WS_2 nanosheet networks with flower-like morphologies on a variety of conducting substrates. The semiconducting WS_2 nanosheets with largely exposed edge sites on flexible carbon fibers enable abundant catalytically active sites, excellent charge transfer, and high permeability to chemicals and biomaterials. Thus, the 3D WS_2-based nano-bio-interface exhibits a wide detection range, high sensitivity and rapid response time for H_2O_2, and is capable of visualizing endogenous H_2O_2 produced in living RAW 264.7 macrophage cells and neurons. First-principles calculations further demonstrate that the enhanced sensitivity of probing H_2O_2 is attributed to the efficient and spontaneous H_2O_2 adsorption on WS_2 nanosheet edge sites. The combined features of 3D WS_2 nanosheet networks suggest attractive new opportunities for exploring the physiological roles of reactive oxygen species like H_2O_2 in living systems.

1. Introduction

The three-dimensional (3D) nano-bio-interface has been attracting substantial research interest in chemistry, nanotechnology and life sciences in recent years.[1] Understanding the interplay of materials and energy at biological interfaces has inspired the rational design of 3D nano-bio-interfaces, which are endowed with advantages and capabilities in developing advanced biological science and technology.[1] Transition metal dichalcogenides (TMDs) are a group of unique 2D materials, owing to their intriguing layer-dependent electronic and optical properties.[2–5] Recent research studies have revealed the possibilities of nano-bio-interface based on TMDs with different morphologies for drug delivery,[6] sensing,[7,8] photothermal materials,[9] electroluminescence[10] and electrocatalysis.[11]

Among many reactive oxygen species (ROS), hydrogen peroxide (H_2O_2) is an important signal messenger molecule that triggers reversible post-translational modifications of downstream targets, such as phosphatases, ion channels, transcription factors and kinases.[12,13] It has also been realized that H_2O_2 plays essential functions in healthy physiological signaling pathways.[14] The capability of fast and sensitive H_2O_2 measurement especially in cellular environments and functions represents attractive advantages for understanding how cells produce, partition and funnel H_2O_2 into specific signaling pathways.[15,16] The use of ultrasmall MoS_2 platelets has recently been reported on the electrochemical detection of hydrogen peroxide (H_2O_2) secreted by living cells.[8] However, the development of the TMD-based nano-bio-interface with sensitive signal monitoring and probing of living cells is still at a very early stage, in which one of the significant challenges is to probe living cells grown on 3D structures that mimic real environments inside tissues. Solving this challenge requires the development of new probing platforms with high interaction interfaces, abundant active sites and easy accessibility, as well as sensitive and selective means for identifying the biosignals derived from cellular activities.[1]

In this work, we demonstrate the fabrication of a 3D flower-like tungsten sulfide (WS_2) nanosheet network with exposed edge sites grown on a large variety of substrates *via* a chemical

[a]*Laboratory of Advanced Materials, Department of Chemistry, Collaborative Innovation Center of Chemistry for Energy Materials, Fudan University, Shanghai 200433, China. E-mail: gfzheng@fudan.edu.cn*
[b]*Key Laboratory of Computational Physical Sciences, Ministry of Education, State Key Laboratory of Surface Physics, and Department of Physics, Fudan University, Shanghai 200433, China*
[c]*Institute of Brain Science and State Key Laboratory of Medical Neurobiology, Fudan University, Shanghai 200032, China*
[d]*Department of Chemistry, College of Science, King Saud University, Riyadh 11451, Saudi Arabia*
[e]*Department of Cardiovascular Surgery, Zhongshan Hospital, Fudan University, Shanghai 200032, China*
†Electronic supplementary information (ESI) available: Additional figures. See DOI: 10.1039/c5nr09236a
‡These authors contributed equally to this work.

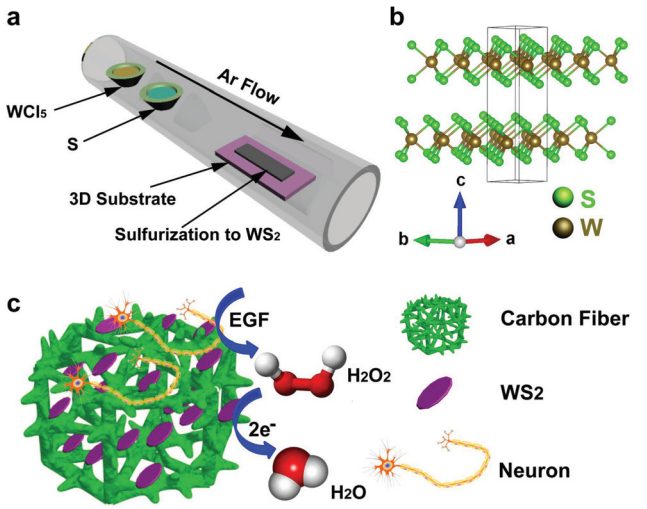

Fig. 1 (a) Schematic diagram of the synthesis setup of WS_2 in a horizontal CVD tube furnace. (b) Layered crystal structure of WS_2. (c) 3D WS_2 for electrochemical sensing of H_2O_2 produced from neurons.

vapor deposition (CVD) approach (Fig. 1a). The strong W–S covalent bonding within the single molecular layers and the weak van der Waals interaction between them give rise to a strong anisotropy (Fig. 1b). As the main electrochemical activity of MoS_2 takes place at its edge planes,[17] the 3D WS_2 nanosheets present high densities of exposed edges and a continuous and highly conductive network, inheriting both the merits of abundant active reactive sites of individual 2D nanostructures and the efficient charge transfer of the 3D network assembly.[18] This 3D WS_2 nanosheet network exhibits excellent catalytic activity towards H_2O_2 reduction, featuring real-time and ultrasensitive detection of H_2O_2. Furthermore, the WS_2-based networks with high bio-compatibility can further be interfaced with living cells for cell culture and detection platform for a variety of cell types, which offers a similar 3D environment for cell growth with large surface areas enhancing the loading capacity, thus enabling direct probing of H_2O_2 production from the cells under various stimulation and signaling. As a proof-of-concept, both the RAW 264.7 macrophage cells and the primary hippocampal neurons directly grown on and interfaced with the 3D WS_2 have been utilized for real-time monitoring of the H_2O_2 production *via* epidermal growth factor (EGF) excitation and different cellular inhibition pathways (Fig. 1c), suggesting the capability of probing the nanomaterial–cell interfaces by the 3D WS_2 sensors.

2. Experimental

2.1 Synthesis of WS_2 nanostructures

Ti foils (0.05 mm thick, ~2 cm^2) were cleaned by sonication in acetone, isopropyl alcohol, and deionized (DI) water for 20 min each, and then dried using nitrogen flow. Recycled tungsten substrates were first etched in aqua regia (3 : 1 concentrated HCl : concentrated HNO_3) for 10 min to remove remnant materials and ensure a consistent reaction substrate. A home-built single-zone CVD reactor consisting of a 1-inch-diameter quartz tube and pressure and gas flow controls was used for the synthesis. In brief, an alumina combustion boat containing 50 mg tungsten chloride (WCl_5, 99.9%) and 200 mg elemental sulfur (99.5%) was placed outside the tube furnace upstream of the prepared tungsten substrates. The reactor was evacuated and flushed three times with argon, and then filled to 770 Torr under an argon flow of 125 sccm and heated to 550 °C. The combustion boat was pushed 1.5 cm into the furnace using a magnet and hydrogen flow was started at 0.75 sccm to initiate the reaction for 20 min. After that, the furnace was cooled naturally under an argon flow.

2.2 Theoretical calculations

First-principles calculations were carried out for structural relaxation and total energy calculation. The basal plane system was simulated by a 4 × 4 WS_2 bilayer with 32 W atoms and 64 S atoms. The vacuum space perpendicular to the WS_2 (001) surface was around 15 Å, which is enough to avoid the interaction between periodic images. A supercell was built with lattice parameter 12.74 × 12.74 × 29.18 $Å^3$. For the nanoribbon calculations, 3× periodicity was applied, and the periodic boundary condition was along a certain direction. The cell built for the ribbon was 9.55 × 47.77 × 18.00 $Å^3$. For the 2S edge, 33 W atoms and 68 S atoms were involved in the calculation. For the 2S2–S edge, 33 W atoms and 71 S atoms were involved in the calculation. For the 3S edge, 33 W atoms and 69 S atoms were involved in the calculation. The ion–electron interaction was treated by the projector augmented-wave (PAW) technique, as implemented in the Vienna ab initio simulation package (VASP). The exchange–correlation potential was treated using the Perdew–Burke–Ernzerhof (PBE) functional. The 3D k-mesh was generated by the using Monkhorst–Pack scheme, where the density of *k*-points was determined by the lattice constant (11 × 11 × 4 $Å^3$ for the bulk WS_2, 3 × 3 × 1 $Å^3$ for the slab model, and 3 × 1 × 1 $Å^3$ for the nanoribbon). The lattice vectors and atomic positions are optimized according to the guidance of atomic forces, with a criterion that requires the calculated force on each atom smaller than 0.01 eV $Å^{-1}$.

2.3 Cell culture

RAW 264.7 macrophage cells (ATCC) were grown in 5% CO_2 in 75 cm^2 flasks containing Dulbecco's modified Eagle's medium with 1% antibiotics and 10% (v/v) fetal bovine serum (FBS) at 37 °C. After growing to 90% confluence, the cells were collected by centrifugation and washed with PBS three times. During the test, a pellet that contained 2 × 10^6 cells was resuspended into 20 mL of phosphate buffer saline (PBS, 0.1 M, pH 7.4) and the mixture was saturated with N_2. As a control group, 60 U mL^{-1} (final concentration) of catalase was added to the solution that contained cells. A potential of −0.25 V (*vs.* Ag/AgCl electrode) was applied to the 3D WS_2 electrode. A 0.3 μM solution of *N*-formylmethionyl-leucyl-phenylalanine (fMLP, 97%, Aldrich) was added into the culture solution after a steady background noise was obtained.

2.4 Electrochemical measurement

The 3D WS_2 served as the working electrode, while a platinum foil electrode and an Ag/AgCl electrode were used as the counter and reference electrodes, respectively. Electrochemical measurements were performed using a CHI660D electrochemical workstation (CH Instrument Inc., China). For the H_2O_2 sensing, the time-dependent conductivity test was carried out in 5 mL of PBS solution at a bias voltage of −0.25 V, with the addition of different concentrations of H_2O_2 in PBS. For the cellular measurement, both RAW 264.7 macrophage cells were incubated with 0.3 μM fMLP (Sigma-Aldrich, USA) for 5 min. For the catalase inhibition, 1 mL of a catalase solution (350 unit mL^{-1}) was added into the cell culture for 30 min, before the addition of fMLP. The measurement of the 3D WS_2 was carried out in the same solution as the cell culture medium. Then 10 μL of the cell culture was injected into the detection solution (5 mL) for the conductivity measurement. In the selectivity test, the superoxide anion ($O_2^{\bullet-}$) was derived from dissolved KO_2 (10 μM) in the DMSO solution. The hypochlorite anion (ClO^-) was supplied by NaClO (10 μM). Typical ROS included $O_2^{\bullet-}$, and ClO^- with 100-fold higher concentrations compared to that of H_2O_2.

2.5 Immunostaining

For immunostaining, the cells were washed three times in phosphate buffer saline (PBS), fixed in 4% paraformaldehyde for 12 min, and permeabilized for 5–15 min with 0.01–0.2% Triton-100 in PBS containing 10% donkey serum. After a brief wash in PBS, the cells were incubated with primary antibodies overnight at 4 °C. The fluorescence signals were visualized with a Nikon A1 confocal microscope (Nikon Instruments Inc., Japan). The neurons in culture were permeabilized with 0.1% Triton-100. All primary antibody dilutions were performed with simple solutions containing only buffer and primary antibody without excess protein blocks or detergents.

3. Results and discussion

3.1 3D WS_2 synthesis

The WS_2 nanosheet arrays were synthesized *via* a chemical vapor deposition (CVD) method, with WCl_5 and sulfur as precursors (see Methods in the ESI†). Scanning electron microscopy (SEM) images display that nanosheet structures can be directly grown on various substrates, including carbon fiber cloths (Fig. 2a and b), Ti foil (Fig. 2c), and nickel foam (Fig. 2d). The nanosheets formed a flower-like morphology on either flat or 3D substrates, which allows maximizing exposure of active sites on the edge of nanosheets. Particularly, carbon fibers (CFs), utilized as a flexible substrate, can load more catalysts than the flat ones, thus contributing to facilitating the catalytic performance per geometric area.[19] In the meantime, carbon fibers display attractive tensile properties, electric conductivity, high thermal and chemical stabilities, and low-cost and are environmentally friendly.[20] Thus, carbon fiber cloths composed of conductive carbon fiber matrix, ~10 μm in diameter, several millimeters in length and ~13 times surface area per geometric area,[19] have been focused on in our work for the fabrication of WS_2-based electrochemical sensors and cell-nanomaterial interfaces.

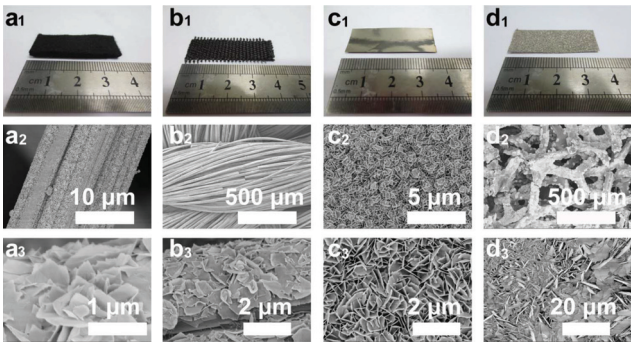

Fig. 2 Representative photographs and SEM micrographs manifesting high density deposition of the flower-like WS_2 nanosheets on (a, b) carbon fibers, (c) Ti foil, (d) nickel foam.

Transmission electron microscopy (TEM) images demonstrate that the individual WS_2 nanosheets have an average edge length of hundreds of nanometers. High-resolution TEM (HRTEM) images reveal highly crystalline multilayered platelets, and the average thickness is below 10 layers (Fig. 3a and b). This ultrathin nanosheet thickness suggests that the crystalline edges contribute to a substantial portion of the crystal structure. The corresponding selected area electron diffraction

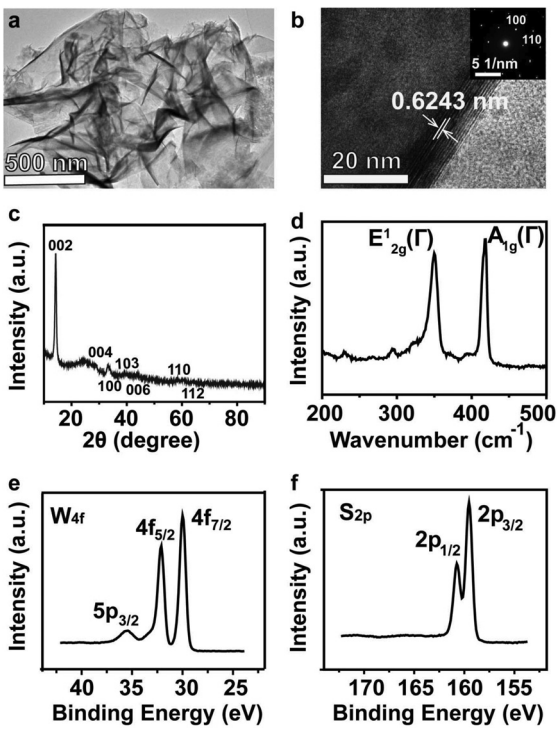

Fig. 3 Characterization of WS_2 nanosheets. (a) TEM, (b) HRTEM, inset: SAED image of WS_2, (c) XRD pattern, (d) Raman spectrum, and (e, f) XPS spectra of WS_2 nanosheets.

(SAED) pattern confirms the single crystalline structure and is indexed to 2H–WS_2 (Fig. 3b, inset). The phase identity of the as-synthesized WS_2 nanostructures is further confirmed by the X-ray diffraction (XRD) pattern (Fig. 3c), in accordance with the 2H phase of WS_2 [Joint Committee on Powder Diffraction Standards (JCPDS) card no. 08-0237].[18] The strong 002 reflection suggests the ordered stacking of 2D nanosheets in the flower-like WS_2 nanostructures. The Raman spectra of the WS_2 nanosheets were recorded by employing 633 nm excitation, and the distinct peaks at 350 and 416 cm^{-1} are assigned to the in-plane M–X vibration mode ($E^1_{2g}(\Gamma)$) and the out-of-plane M–X vibration mode ($A_{1g}(\Gamma)$), respectively (Fig. 3d),[21] further confirming the 2H phase crystal structure.[18] The significant proportion of the A_{1g} mode in the spectrum indicates the nanosheets are terminated by edges on the surface,[19] as the edge-terminated two dimensional dichalcogenides (MX_2) were grown in such a way that the van der Waals layers were aligned vertically to substrates. X-ray photoelectron spectroscopy (XPS) measurements of the samples display two intensive peaks around 30 and 32 eV, attributed to W $4f_{7/2}$ and W $4f_{5/2}$, respectively, and a weak peak around 36 eV for W $5p_{3/2}$ (Fig. 3e).[22] The dual peaks around 160 eV correspond to S $2p_{3/2}$ and $2p_{1/2}$, respectively (Fig. 3f).

3.2 Electrocatalytic activity toward the reduction of H_2O_2

The electrocatalytic activity of the WS_2/carbon fiber was first explored in PBS toward the reduction of H_2O_2 in PBS (0.1 M, pH = 7.4) with the protection of N_2. In the absence of H_2O_2, almost no redox peaks are recorded on either the blank carbon fiber or the WS_2/carbon fiber electrode (Fig. S1†). On the addition of 5 mM H_2O_2, the reduction current increases significantly, with the peak position around −0.25 V. The H_2O_2 detection of the WS_2 nanosheet networks was then examined by a chronoamperometry ($i - t$) method under neutral conditions (0.1 M PBS, pH 7.4, see Methods in the ESI†). The carbon fiber grown with WS_2 nanosheet networks was used as the working electrode, and a Pt wire and Ag/AgCl were used as the counter and reference electrodes, respectively. A low and constant potential of −0.25 V *versus* Ag/AgCl was applied to the electrochemical sensor, which can lead to a clear current response but also avoid other possible electrochemical side reactions such as water splitting.[23] Amperometric responses of the 3D WS_2 nanosheet network electrodes on successive addition of 10 μM of H_2O_2 were acquired in 0.1 M PBS (pH 7.4) at an applied potential of −0.25 V (Fig. 4a). With the delivery of different concentrations of H_2O_2 at intervals into the electrochemical cell, the WS_2 nanosheet networks respond quickly at each injection and reach a new current equilibrium within a few seconds (Fig. 4a). The lowest detection limit of H_2O_2 is recorded as ~2 nM, with a signal-to-noise ratio of >2 (Fig. 4b), comparable to or exceeding most of the recently reported H_2O_2 sensors (Table S1 in the ESI†).[24,25] This fast sensor response can be attributed to the largely distributed active sites and a high surface area of the 3D WS_2 nanosheet networks, as well as the rapid adsorption and reduction of H_2O_2 on the WS_2 surface. The summarized concentration dependence plot (Fig. 4c) indicates a wide dynamic detection range and high sensitivity. As control, the injections of several interference molecules, such as metal ions, amino acids (Fig. 4d) and other typical ROS including $O_2^{\bullet-}$ and ClO^- with 100-fold concentration compared with that of H_2O_2 (Fig. S2†), do not result in an observable signal, confirming the good selectivity of the sensor.

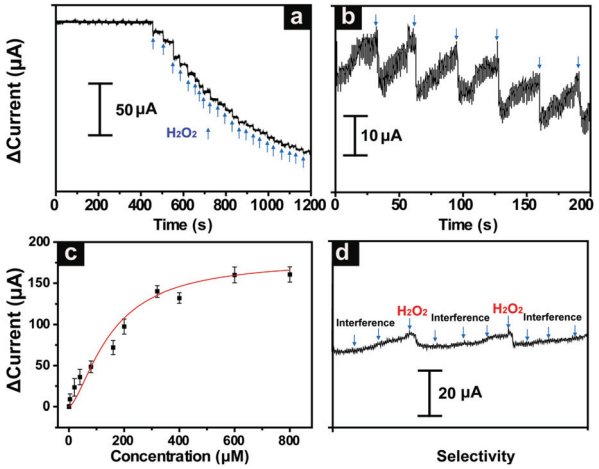

Fig. 4 H_2O_2 sensing performance of 3D WS_2 nanosheet-networks. (a) Amperometric response ($i - t$) of the 3D biosensor loaded with WS_2 nanosheets to the consecutive injection of different concentrations of H_2O_2 in PBS solution (0.1 M, pH 7.4) at a constant potential −0.25 V *versus* Ag/AgCl electrode. (b) A closer look at the amperometric response with the addition of 2 nM H_2O_2. (c) Concentration dependence of the response of 3D WS_2 nanosheet networks at H_2O_2 concentrations. (d) Current response of the 3D biosensor to the injection of H_2O_2, as well as interferences including metal ions and amino acids.

First-principles calculations were performed to interpret the excellent H_2O_2 sensitivity of the WS_2 nanosheet networks, as one of the most unique features of the flower-like WS_2 is the substantial amount of exposed edges in the structure. To quantitatively correlate the sensitivity with microscopic structures, models for both plane and edge were built in atomic scale precision, and the adsorption energies between H_2O_2 on the WS_2 basal plane or edge positions were calculated. The basal plane of WS_2 was constructed with a 4× periodicity (Fig. 5a). The H_2O_2 adsorption energy is defined as $\Delta E_{H_2O_2} = E_{WS_2+H_2O_2} - E_{WS_2} - E_{H_2O_2}$, where $E_{WS_2+H_2O_2}$ is the total energy for the WS_2 system with H_2O_2 adsorbed on the surface, E_{WS_2} is the total energy for the WS_2 surface and $E_{H_2O_2}$ is the energy for the H_2O_2 molecule in the gas phase. The $\Delta E_{H_2O_2}$ obtained from the ground state calculation is −0.02 eV and is not sensitive to the orientations of the H_2O_2 molecule, indicating that the adsorption of H_2O_2 onto the WS_2 surface is a spontaneous process.

The nanoribbon models of the non-metallic transition metal dichalcogenides were then applied to study the edge effect.[26] Note that the ribbons have two edges: the transition metal (W) edge and the sulfur (S) edge, while the transition metal edge is also terminated by S atoms from experimental observation. As the transition metal edge is more often

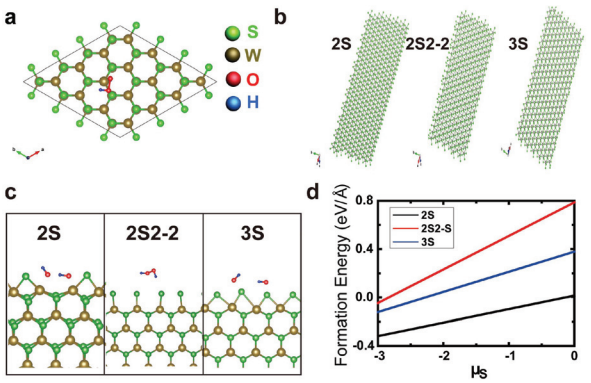

Fig. 5 DFT calculations. (a) Structural model for computational simulation of H_2O_2 adsorption on the surface of 2H–WS_2. Green, brown, red and blue spheres represent the S, W, O and H atoms. (b) Illustration of the nanoribbon model used to simulate the edge of flower-like WS_2. Three kinds of reconstructions of the edge are built, denoted as 2S, 2S2–2 and 3S. (c) Adsorption of H_2O_2 on the WS_2 edge. (d) Formation energy of the WS_2 edge for the three kinds of WS_2 edges.

observed in experiments,[27] the adsorption of H_2O_2 on the tungsten (W) edge is evaluated. These non-metallic nanoribbons satisfy the electron counting rule (ECR), so they are all in 3× periodicity (Fig. 5b).[26] For the 2S edge, two S atoms are added to the W edge applying the ECR. For the 2S2–2 edge, a pair of S atoms and a S adatom is added to the 2S edge. For the 3S edge, three S atoms are added to the W edge. The models of H_2O_2 on these three WS_2 edges were demonstrated (Fig. 5c). Using the same method above, the adsorption energies ($\Delta E_{H_2O_2}$) of H_2O_2 on the 2S, 2S–2 and 3S edges were calculated as −4.58, −0.03 and 0.136 eV, respectively. It can be seen that the different termination of the W edge exhibits drastically different properties of H_2O_2 adsorption. To determine which edge effect is dominant, the formation energy of the various edges was calculated as a function of S chemical potential (Fig. 5d). The chemical potential is subject to the constraint $\mu_W + 2\mu_S < \Delta H_{(WS_2)}$, where $\Delta H_{(WS_2)}$ is the enthalpy of formation of WS_2, and μ_S is the chemical potential of S referring to the S_2 molecule. The formation energy was calculated as the difference in total energies between the nanoribbon and the primitive WS_2 cell, and the energies were normalized to per ribbon length. The more negative the energies, the more stable the nanoribbon. Despite the change of chemical potential, the 2S edge of WS_2 is always the most stable one, on which the adsorption of H_2O_2 takes place most easily. These calculations explain the high sensitivity to the H_2O_2 molecule of the edge-rich flower-like WS_2.

3.3 Tracking of H_2O_2 from living cells

The constructed 3D WS_2 nanosheet network sensor was then applied for the real-time tracking of H_2O_2 released by living RAW 264.7 macrophage cells. SEM images show that RAW 264.7 cells were well grown on top of WS_2 nanosheets over carbon fiber cloths (Fig. 6a and b), which can be attributed to both the low toxicity of WS_2 observed in previous experiments[6]

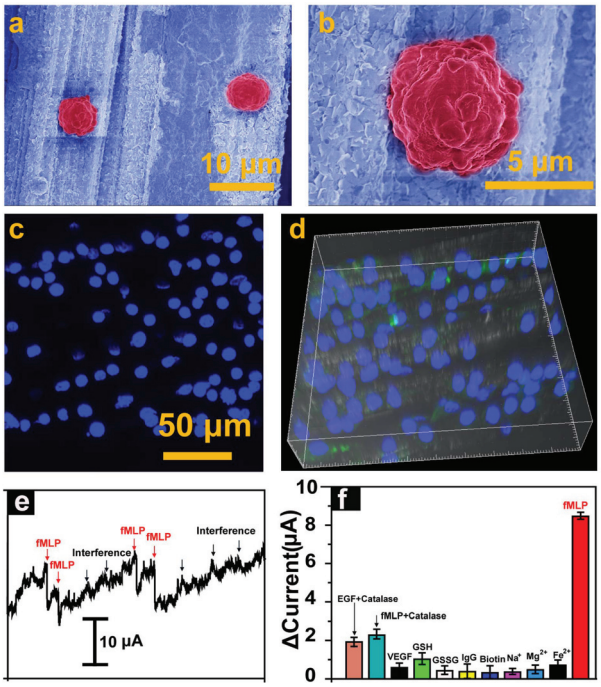

Fig. 6 3D cell culture and electrical sensing on a carbon fiber cloth. (a, b) SEM images of RAW 264.7 cells grown on the carbon fiber cloth. RAW 264.7 cells were displayed in pseudo color. (c, d) Fluorescence images of cells labeled with 4,6-diamidino-2-phenylindole (DAPI), phalloidin, and fluorescein isothiocyanate for cell morphology visualization on the carbon fiber cloth. (e) Amperometric responses of the WS_2 nanosheet electrodes to the addition of 0.3 μM fMLP with Raw 264.7 cells in the N_2-saturated 0.1 M PBS at −0.25 V *versus* the Ag/AgCl electrode. (f) Summary of the selectivity of the 3D WS_2 sensors for various analytes.

and 3D cell growth environments on the WS_2 nanosheet networks/carbon fibers. Bright field and confocal fluorescence images of the RAW 264.7 macrophage cells, cultured for 72 h on top of the WS_2 nanosheets, exhibit that the cells preserved normal morphologies and functions (Fig. 6c and d), thus allowing for direct H_2O_2 detection by the WS_2 nanosheet sensors beneath. The H_2O_2 released from the living RAW 264.7 cells was triggered by adding *N*-formylmethionyl leucyl phenylalanine (fMLP), which leads to H_2O_2 release that can resemble the oxidative metabolism most likely to be encountered *in vivo*.[28] When 0.3 μM fMLP solution was added to the cell-WS_2 nanosheet sensor culture, an obvious current change corresponding to 2 nM H_2O_2 was recorded, while no signal was generated if the cells were not treated with fMLP (Fig. 6e). Common interferences such as vascular endothelial growth factor (VEGF) and metal ions were also added to test the selectivity of the WS_2 nanosheet biosensor, which demonstrated negligible responses (Fig. 6f). In addition, when catalase, an enzyme that catalytically decomposes H_2O_2,[29] was mixed with fMLP and added into the solution, the current change was reduced to almost negligible.

To verify whether these 3D WS_2 can be used to visualize natural cellular H_2O_2 generation, the relationships between physiological H_2O_2 production and growth factor signaling

were further probed,[30] in which the direct interfacing of neural cells to the WS_2 nanosheet networks was fabricated. SEM images of these rat hippocampal neurons grown on the WS_2 nanosheet surface exhibit clear cell bodies, axonal spreading and extension of dendrites (Fig. 7a and b). Confocal microscopy images of 4,6-diamidino-2-phenylindole (DAPI) staining identify the cell nuclei (blue) (Fig. 7c), and the MAP2 staining shows neurons with a spatially interconnected dendrite network that spread out over the nanosheet surface (Fig. 7d). NeuN, a nuclear protein was utilized as a neuronal marker.[31] The NeuN immunostaining was remarkably localized to the nucleus, albeit some neurons manifested perinuclear staining as well (Fig. 7e). The live neurons cultured on the 3D WS_2 were activated with a physiologically relevant dose of growth factor (500 ng mL^{-1} EGF for 15 min at 37 °C), and showed high signal relative to pre-stimulation levels (Fig. 7f, black and red bar). Then 3D WS_2 were employed to probe the molecular pathway of EGF mediated H_2O_2 production in conjunction with chemical inhibitors. The EGF-stimulated generation of H_2O_2 was attenuated by the inhibitor of the EGFR kinase domain (PD153035, 100 mM, Fig. 7f, green bar), the inhibitor of phosphatidylinositol-3-OH kinase (wortmannin, 100 mM, Fig. 7f, blue bar), the inhibitor of NO synthase (NSC23766, 100 mM, Fig. 7f, light blue bar), and the inhibitor of Nox (apocynin, 100 mM, Fig. 7f, pink bar), which are indicated by the absence of the observable electrochemical signal from the WS_2 nanosheet sensor. Taken together, the results demonstrate that 3D WS_2 are capable of detecting natural signaling levels of H_2O_2 generated by living cells and can be used to map molecular pathways associated with H_2O_2 production.

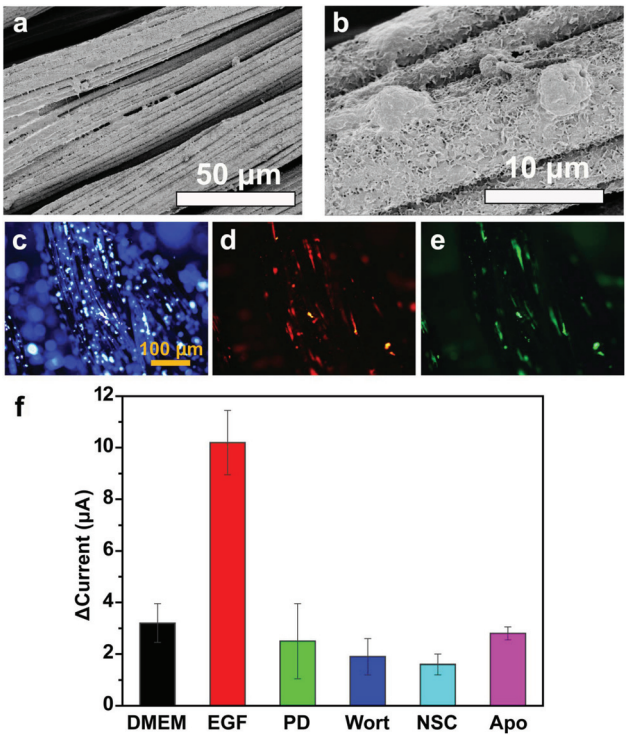

Fig. 7 H_2O_2 and growth factor signaling in living neurons. (a, b) SEM images of the morphology of hippocampal neurons on nanosheets. (c–e) Fluorescence images of the fixed hippocampal neurons cultured on the WS_2 nanosheets, using (c) DAPI as the nucleus marker for cell counting, (d) Map2 as the membrane marker for the cell morphology, and (e) NeuN for neuron protein visualization on substrates. (f) Summary of the current changes recorded from a WS_2 sensor interfaced with neurons for various treatments. DMEM: Dulbecco's modified Eagles' medium. EGF: epidermal growth factor. PD: PD153035. Wort: wortmannin. NSC: NSC2376. Apo: apocynin.

4. Conclusions

We have developed a WS_2 nanosheet network grown on 3D conducting substrates as an efficient H_2O_2 sensing platform, by exposing the abundant edge sites of the nanostructures. The formed 3D networks serve as both an excellent growth substrate for cell culture, and a unique electrochemical measurement platform for H_2O_2 released from cells. As a proof-of-concept, these 3D WS_2 nanosheets afford specific and sensitive detection of H_2O_2 in aqueous solution and in living cells. The ability to specifically monitor H_2O_2 in living cells such as RAW 264.7 cells and neurons at signaling concentrations opens new avenues for the rapidly expanding field of biology, and suggests further potential for probing transient molecules and signaling of short duration and lifetime.[32]

Conflict of interest

The authors declare no competing financial interest.

Acknowledgements

We thank the following funding agencies for supporting this work: the National Key Basic Research Program of China (2013CB934104), the Natural Science Foundation of China (21322311, 21473038), the Science and Technology Commission of Shanghai Municipality (14JC1490500), the Program for Professor of Special Appointment (Eastern Scholar) at the Shanghai Institutions of Higher Learning, and the Collaborative Innovation Center of Chemistry for Energy Materials (2011-iChem). Y. Q. acknowledges the support of Wang-Dao Undergraduate Research Funding of Fudan University. The authors extend their sincere appreciation to the Deanship of Scientific Research at King Saud University for funding the prolific research group (PRG-1436-14).

References

1 X. Liu and S. Wang, *Chem. Soc. Rev.*, 2014, **43**, 2385–2401.
2 X. Duan, C. Wang, J. C. Shaw, R. Cheng, Y. Chen, H. Li, X. Wu, Y. Tang, Q. Zhang, A. Pan, J. Jiang, R. Yu, Y. Huang and X. Duan, *Nat. Nanotechnol.*, 2014, **9**, 1024–1030.

3 R. Cheng, D. Li, H. Zhou, C. Wang, A. Yin, S. Jiang, Y. Liu, Y. Chen, Y. Huang and X. Duan, *Nano Lett.*, 2014, **14**, 5590–5597.
4 L. Zhang, K. Liu, A. B. Wong, J. Kim, X. Hong, C. Liu, T. Cao, S. G. Louie, F. Wang and P. Yang, *Nano Lett.*, 2014, **14**, 6418–6423.
5 X. Huang, Z. Zeng, S. Bao, M. Wang, X. Qi, Z. Fan and H. Zhang, *Nat. Commun.*, 2013, **4**, 1444.
6 L. Cheng, J. Liu, X. Gu, H. Gong, X. Shi, T. Liu, C. Wang, X. Wang, G. Liu, H. Xing, W. Bu, B. Sun and Z. Liu, *Adv. Mater.*, 2014, **26**, 1886–1893.
7 D. Sarkar, W. Liu, X. Xie, A. C. Anselmo, S. Mitragotri and K. Banerjee, *ACS Nano*, 2014, **8**, 3992–4003.
8 J. Tang, J. Li, Y. Zhang, B. Kong, Yiliguma, Y. Wang, Y. Quan, H. Cheng, A. M. Al-Enizi, X. Gong and G. Zheng, *Anal. Chem.*, 2015, **87**, 6703–6708.
9 T. Liu, C. Wang, X. Gu, H. Gong, L. Cheng, X. Shi, L. Feng, B. Sun and Z. Liu, *Adv. Mater.*, 2014, **26**, 3433–3440.
10 D. Li, R. Cheng, H. Zhou, C. Wang, A. Yin, Y. Chen, N. O. Weiss, Y. Huang and X. Duan, *Nat. Commun.*, 2015, **6**, 7509.
11 J. Li, Y. Wang, T. Zhou, H. Zhang, X. Sun, J. Tang, L. Zhang, A. Al-Enizi, Z. Yang and G. Zheng, *J. Am. Chem. Soc.*, 2015, **137**, 14305–14312.
12 B. Dickinson and C. Chang, *Nat. Chem. Biol.*, 2011, **7**, 504–511.
13 B. Dickinson, J. Peltier, D. Stone, D. Schaffer and C. Chang, *Nat. Chem. Biol.*, 2011, **7**, 106–112.
14 B. Dickinson, V. Lin and C. Chang, *Nat. Protoc.*, 2013, **8**, 1249–1259.
15 V. Lin, A. Lippert and C. Chang, *Proc. Natl. Acad. Sci. U. S. A.*, 2013, **110**, 7131–7135.
16 J. Chan, S. Dodani and C. Chang, *Nat. Chem.*, 2012, **4**, 973–984.
17 J. Bai and X. Jiang, *Anal. Chem.*, 2013, **85**, 8095–8101.
18 M. Lukowski, A. Daniel, C. English, F. Meng, A. Forticaux, R. Hamers and S. Jin, *Energy Environ. Sci.*, 2014, **7**, 2608–2613.
19 H. Wang, Z. Lu, D. Kong, J. Sun, T. Hymel and Y. Cui, *ACS Nano*, 2014, **8**, 4940–4947.
20 K. Xu, F. Wang, Z. Wang, X. Zhan, Q. Wang, Z. Cheng, M. Safdar and J. He, *ACS Nano*, 2014, **8**, 8468–8476.
21 J. Yu, H. Lee, S. Hong, D. Kong, H. Lee, H. Wang, F. Xiong, S. Wang and Y. Cui, *Nano Lett.*, 2015, **15**, 1031–1035.
22 J. Duan, S. Chen, B. Chambers, G. Andersson and S. Qiao, *Adv. Mater.*, 2015, **27**, 4234–4241.
23 T. Wang, H. Zhu, J. Zhuo, Z. Zhu, P. Papakonstantinou, G. Lubarsky, J. Lin and M. Li, *Anal. Chem.*, 2013, **85**, 10289–10295.
24 B. Dickinson and C. Chang, *J. Am. Chem. Soc.*, 2008, **130**, 9638–9639.
25 M. Chang, A. Pralle, E. Isacoff and C. Chang, *J. Am. Chem. Soc.*, 2004, **126**, 15392–15393.
26 M. Lucking, J. Bang, H. Terrones, Y. Sun and S. Zhang, *Chem. Mater.*, 2015, **27**, 3326–3331.
27 J. Lauritsen, J. Kibsgaard, S. Helveg, H. Topsøe, B. Clausen, E. Lægsgaard and F. Besenbacher, *Nat. Nanotechnol.*, 2007, **2**, 53–58.
28 X. Sun, S. Guo, Y. Liu and S. Sun, *Nano Lett.*, 2012, **12**, 4859–4863.
29 A. Lippert, G. Van de Bittner and C. Chang, *Acc. Chem. Res.*, 2011, **44**, 793–804.
30 E. Miller, O. Tulyathan, E. Isacoff and C. Chang, *Nat. Chem. Biol.*, 2007, **3**, 263–267.
31 E. Mezey, K. Chandross, G. Harta, R. Maki and S. McKercher, *Science*, 2000, **290**, 1779–1782.
32 J. Tang, J. Li, P. Da, Y. Wang and G. Zheng, *Chem. – Eur. J.*, 2015, **21**, 11288–11299.

